Journal of
Applied Crystallography
ISSN 0021-8898

Received 16 August 2006
Accepted 14 March 2007

X-ray studies of the self-organized structure formed by 1,2-bis(4′-*n*-alkoxybenzoyl)hydrazine (BABH-*n*) homologues. 1. *Ia*3*d*-gyroid structure

Shoichi Kutsumizu,[a]* Hiroyuki Mori,[a] Machiko Fukatami[a] and Kazuya Saito[b]

[a]Department of Chemistry, Faculty of Engineering, Gifu University, Gifu 501-1193, Japan, and [b]Department of Chemistry, Graduate School of Pure and Applied Sciences, University of Tsukuba, Tsukuba, Ibaraki 305-8571, Japan. Correspondence e-mail: kutsu@gifu-u.ac.jp

The cubic (Cub) phase structure of a thermotropic mesogen 1,2-bis(4′-*n*-alkoxybenzoyl)hydrazine (BABH-*n*, where *n* is the number of C atoms in the aliphatic tail) was examined by small-angle X-ray scattering. The BABH-*n* system exhibits two types of Cub phases, *Ia*3*d* type and *Im*3*m* type. In the phase diagram as a function of the tail length (*n*) the *Im*3*m*-Cub phase region (*n* = 13–16) was sandwiched by two *Ia*3*d*-Cub phase regions with *n* < 13 and *n* > 16. On the basis of the triply periodic minimal surface (TPMS) picture, the *Ia*3*d* and *Im*3*m* structures are described by the gyroid (G) and doubled-P (PP) surfaces, respectively. In this paper we focused attention on the internal structure of the *Ia*3*d*-Cub phase at the molecular level. By examining how the relative intensity of the 220 reflection with respect to the 211 reference peak varies with *n*, we have successfully determined the position of the aliphatic tails, which are located on the G-TPMSs. As far as we know, this is the first approach to clarifying the internal structure of the thermotropic *Ia*3*d*-Cub phase. The usefulness of the systematic studies with respect to the tail length *n* has also been demonstrated.

1. Introduction

Among various liquid-crystalline (LC) phases, thermotropic cubic (Cub) phases of bicontinuous type are of much interest in that both local mobility and a three-dimensionally periodic molecular arrangement are realised by relatively simple rod-like molecules (Diele & Göring, 1998; Diele, 2002; Kutsumizu, 2002; Impéror-Clerc, 2005). In lyotropic LC systems, the cubic phase is relatively well known and observed in the region where the volume fraction ϕ of one of the two chemically incompatible components (polar or aliphatic) deviates slightly from $\phi = 0.5$; at $\phi = 0.5$ the lamellar phase is stabilized. The most frequently observed Cub phases have the space group *Ia*3*d*. To describe the structure, the most common approach is based on the assumption that the curved layers made of either a polar or aliphatic medium decorate the triply periodic minimal surfaces (TPMSs); the TPMS corresponding to space group *Ia*3*d* is the G surface (or gyroid) (Schoen, 1970). (This surface is shown later in Fig. 2).

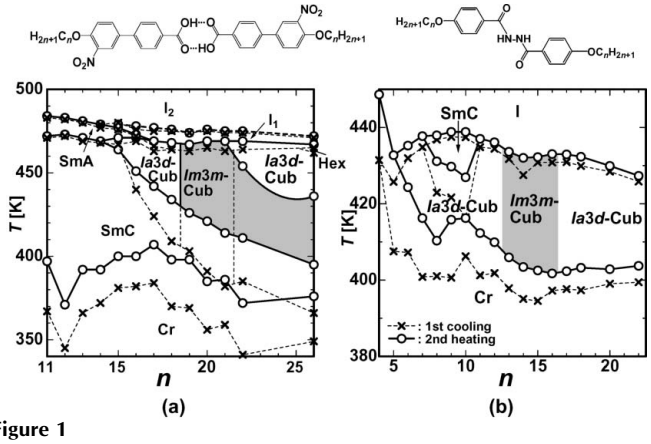

Figure 1
Phase diagrams of two thermotropic cubic mesogens. (a) ANBC-*n* (Kutsumizu, 2002: Cr, crystal; SmC/A, smectic C/A; Cub, cubic; I_1 and I_2 are a structured liquid and the normal isotropic liquid, respectively). (b) BABH-*n* (Mori *et al.*, 2006). Their chemical structures are also given above the diagrams.

The Cub phase formation in the thermotropic LC systems is also understood qualitatively in the same manner. Tardieu & Billard (1976) investigated the *Ia*3*d*-Cub phase in the *n* = 16 homologue of a well known thermotropic mesogen 4′-*n*-alkoxy-3′-nitrobiphenyl-4-carboxylic acid [denoted as ANBC-*n*, where *n* is the number of C atoms in the alkoxy group; the chemical structure is shown in Fig. 1(a)], where, instead of the polar and aliphatic parts segregating in the lyotropic systems, microsegregation between the aromatic core and aliphatic chain parts of the constituent molecules takes place (quasi-binary picture) (Saito *et al.*, 1998; Sato *et al.*, 1999; Saito & Sorai, 2002).

One of the common techniques used to identify the structure of the Cub phase is small-angle X-ray scattering (SAXS). The symmetry of the structure, *i.e.* the space group, can be relatively easily identified on the basis of the relative positions of the Bragg peaks (using the extinction rules). The internal structure, however, can only be resolved by quantitative analysis of the scattering intensities. Such a path to reach the final goal is at first glance very clear, but actually it is very difficult to get the final answer along this route. One of the reasons is that due to their spatially and dynamically disordered

nature only a few peaks are observed, which are not enough to reconstruct the three-dimensional electron-density map. One also encounters another complicated situation: as Luzzati *et al.* (1968) and Clerc & Dubois-Violette (1994) reported, the SAXS patterns of some lyotropic Cub phases were reproduced by using a structural model where the aliphatic tails are placed on the TPMS (inverse phase), but the reverse situation, *i.e.* where the polar group is placed on the TPMS (direct phase), is equally plausible for intensity fitting. This problem is also related to the fact that the volume fraction ϕ of one component for the Cub phase formation is close to and does not deviate strongly from 0.5, usually around 0.4 or around 0.6. Thus, from the observed scattering pattern, it is not so easy to differentiate between the two possibilities for the internal structure of aliphatic tails on the TPMS or polar groups on the TPMS.

In the thermotropic LC systems, the above problem becomes more crucial because unlike the change in volume fraction at a constant temperature, we are not able to precisely predict the temperature effect on the two parts (core and chain). Thus, although the *Ia*3*d*-Cub structure is usually understood in terms of the G-TPMS, even for such a well known phase, the internal structure at the molecular level is not completely understood and it is not certain which part (core or chain) of the thermotropic LC molecule is located on the G-TPMS.

In our previous investigations of the ANBC-*n* series, it was revealed that systematic studies with respect to the alkoxy chain length *n* are useful and provide valuable information on the phase behavior including the Cub phases (Kutsumizu *et al.*, 1994, 1999; Kutsumizu, Morita, Ichikawa *et al.*, 2002). As shown in the phase diagram of Fig. 1(a), the Cub phase region contained, in addition to the *Ia*3*d*-Cub phase, another type, an *Im*3*m*-Cub phase. This phase, which is probably specific to thermotropic LC systems, is a tricontinuous type (Kutsumizu, Morita, Yano & Nojima, 2002; Saito & Sorai, 2002), not a micellar type with the same symmetry as usually seen in the lyotropic LC and block copolymer systems.

Here we report some results on a similar thermotropic Cub mesogen, 1,2-bis(4′-*n*-alkoxybenzoyl)hydrazine [BABH-*n*; Fig. 1(b)]. Since in the ANBC-*n* system hydrogen-bonded dimers are the basic units constructing the self-organized structures (Kutsumizu *et al.*, 1997), the chemical structures of the two systems BABH-*n* and ANBC-*n* are common in that they are composed of a rigid aromatic core at the center and a flexible aliphatic tail at each end. As easily expected from the similarity of the molecular structure, the BABH-*n* system shows a phase diagram very similar to that of the ANBC-*n* system, as shown in Fig. 1 (Mori *et al.*, 2006, and some new results are also added). Owing to limited space in this paper, after briefly mentioning the two types of Cub phases of the BABH-*n* system, we focus attention on the internal structure of the *Ia*3*d*-Cub phase. By examining the SAXS patterns as a function of the alkoxy chain length *n*, we have successfully determined the position of the aliphatic parts within the Cub structure. As far as we know, this is the first approach of this type in the thermotropic Cub systems.

2. Experimental

The preparation route of the BABH-*n* compounds was basically the same as used previously (Schubert *et al.*, 1978). Phase transition temperatures were determined by differential scanning calorimetry (DSC) and polarizing optical microscopy (POM). The POM photos were also used for identification of the phase type, together with the SAXS patterns.

The SAXS measurements were made using a Rigaku NANO-Viewer IP system. Cu $K\alpha$ radiation (wavelength λ = 0.154 nm) was focused with a confocal max-flux (CMF) mirror and collimated into the sample capillary placed in a heated cell using a three-slit system. The scattered X-rays were recorded on a two-dimensional imaging plate (IP: Fuji Film BAS-IP SR 127) camera with an effective area of 11.5 × 11.5 cm^2, and the distance between the sample and the IP was 45 or 67 cm. After the absence of preferred orientation was ascertained, the intensities were radially integrated and averaged, and redistributed when converting the pixel number into the corresponding scattering angle 2θ to produce a circularly averaged pattern. After the background scattering was subtracted from the Lorentz-corrected intensities, the resultant intensities $I(2\theta)$ were integrated for each reflection as $I(hkl) = \int I(2\theta)\, \mathrm{d}(2\theta)$ and corrected for multiplicity (Garstecki & Hołyst, 2002*b*), which can be related to the structure factors [denoted as $F(hkl)$ for the hkl reflection]. In the final part of this paper, we discuss the internal structure of the *Ia*3*d*-Cub phase at the molecular level, using the intensity ratios of two major reflections, 211 and 220, as a function of the alkoxy chain length *n*.

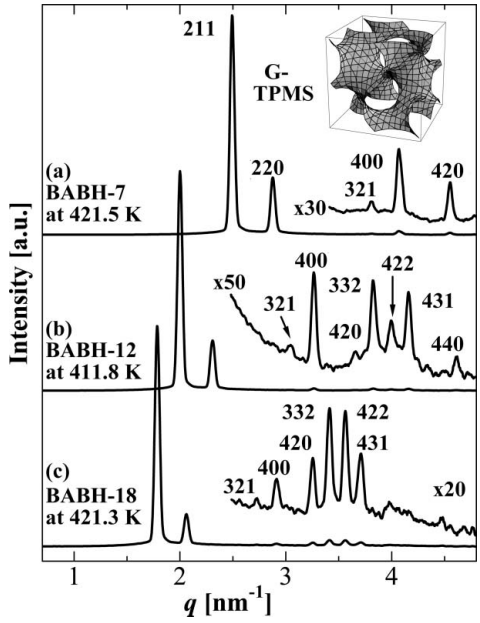

Figure 2
SAXS patterns of the *Ia*3*d* phases for BABH-*n* homologues with *n* = 7, 12 and 18, where the Miller index *hkl* is given for each reflection and the intensities are normalized with respect to that of the 211 reflection. In the upper right-hand corner an illustration of the G-TPMS is also shown.

3. Results and discussion

Fig. 2 shows the SAXS patterns of the *Ia*3*d* phases for BABH-*n* homologues with *n* = 7, 12 and 18. Here, the intensity is expressed as a function of the modulus of scattering vector q [= $(4\pi/\lambda)\sin\theta$] and the background scattering is already subtracted. In Fig. 2(a) for BABH-7, five peaks are seen with the following ratios of reciprocal spacings: $3^{1/2}$: $4^{1/2}$: $7^{1/2}$: $8^{1/2}$: $10^{1/2}$. Since the ratio $7^{1/2}$ is not compatible with any cubic lattice, the sequence of numbers must be doubled and the ratios obtained are $6^{1/2}$: $8^{1/2}$: $14^{1/2}$: $16^{1/2}$: $20^{1/2}$, corresponding to the Miller indices 211, 220, 321, 400 and 420. Reflections with lower indices 100, 110, 111, 200 and 210 are all absent. Since BABH-7 is achiral, the extinction rule observed matches the space group *Ia*3*d* (hkl with $h + k + l = 2n$, $0kl$ with $k = 2n$ and $l = 2n$, hhl with $2h + l = 4n$ and $00l$ with $l = 4n$ are observable, where n = integer and h, k and l are permutable) (*International Tables for Crystallography*, 1989). The same conclusion

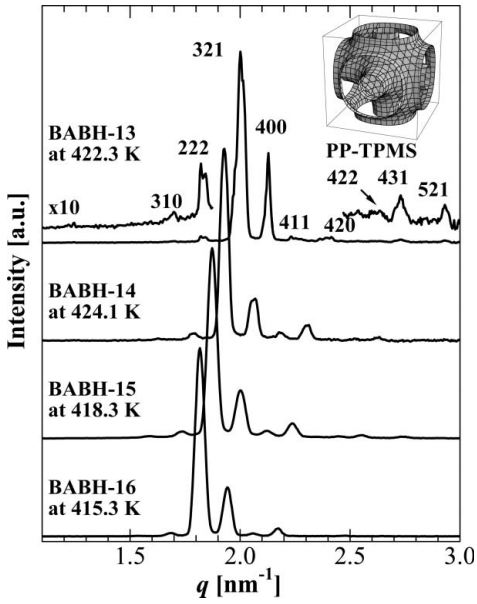

Figure 3
SAXS patterns of the *Im*3*m* phases for BABH-*n* homologues with n = 13–16, where the intensities are normalized with respect to that of the 321 reflection. In the upper right-hand corner an illustration of the PP-TPMS is also shown.

was obtained for BABH-12 [Fig. 2(b)] and BABH-18 [Fig. 2(c)]. Comparing the three *Ia*3*d*-Cub phase patterns, the relative intensity of the 220 reflection with respect to the 211 reflection decreases with increasing n.

Fig. 3 collects the SAXS patterns of the *Im*3*m* phase, where many more reflections are seen. For the four homologues, the Miller indices hkl all satisfy $h + k + l = 2n$ (n = integer), without showing any other systematic rules. Six space groups of the cubic system match this condition and the most symmetric case is *Im*3*m* (*International Tables for Crystallography*, 1989). In the case of two thermotropic systems, the space group was examined in detail and determined to be *Im*3*m* (Zeng *et al.*, 2005). Thus, the space group *Im*3*m* was chosen as the most probable one for the present system. In the phase diagram, the *Im*3*m*-Cub region is in between two *Ia*3*d*-Cub regions [see Fig. 1(b)].

The internal structure of the *Im*3*m*-Cub phase long remained unknown, but recently we have revealed that a suitable structure for this phase is a PP-type TPMS from X-ray studies of the ANBC-*n* system (Kutsumizu, Morita, Yano & Nojima, 2002; Saito & Sorai, 2002). A schematic picture is given in the upper right of Fig. 3. The PP-type TPMS itself was proposed by Schwarz & Gompper (1999)

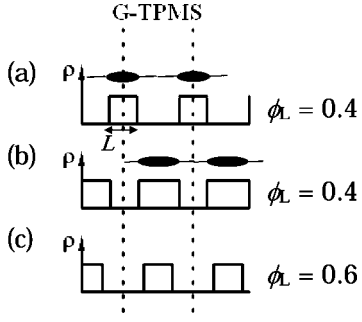

Figure 4
Examples of three electron-density profiles and their relationship to the G-TPMS. Profile (a) represents 'core on TPMS', and (b) and (c) represent 'chain on TPMS'.

and the experimental basis for this suggestion is that the increment of the lattice parameter *a versus n* for the *Im*3*m*-Cub phase is about twice as large as that for the *Ia*3*d*-Cub phase; the number of TPMSs intersecting the face diagonal line per unit cell is doubled in the former phase when compared with the latter (Kutsumizu, Morita, Yano & Nojima, 2002). Very recently, Zeng *et al.* (2005) reported a more sophisticated model by analyzing single-domain diffraction patterns. Although they did not say so, it can be said that, broadly speaking, their model is essentially identical with our model (Kutsumizu, Morita, Yano & Nojima, 2002; Saito & Sorai, 2002), except for the detailed structure such as the octahedral connection of rods at the body center and eight corners of the Cub lattice.

Detailed discussion about the internal structure of the *Im*3*m*-Cub phase is beyond the scope of this paper and here we only mention two points. The intensity variation with q is very similar to that observed for the ANBC-*n* system and other thermotropic *Im*3*m*-Cub phases, which suggests that the same type of structure as mentioned above is formed in the *Im*3*m*-Cub phase of this system. The detailed structure, however, is still unknown, especially concerning the core position with regard to the TPMS.

The main subject of this paper is to determine the internal structure of the *Ia*3*d*-Cub phase at the molecular level. The key work was provided by Garstecki & Hołyst (2000, 2002*a*,*b*). They employed a two-density-level model and assumed that the electron density varies as a step function (as shown in Fig. 4) when going away from the periodic surface. The volume fraction of the layer region decorating the surface with a thickness of L was calculated and denoted as ϕ_L. It was revealed that the relative intensity of the 220 reflection with respect to the 211 reflection (reference peak) decreases when increasing ϕ_L, for example, when the system is changed from Fig. 4(b) to (c). Here, an important point is that the distance between the two neighboring periodic surfaces (which is related to the lattice dimension a) or the contrast of the electron density $|\Delta\rho|$ between the two components itself does not influence the pattern; the 'core on TPMS' model in Fig. 4(a) and 'chain on TPMS' model in Fig. 4(b) are indistinguishable from their scattering patterns (the Babinet principle). However, by examining the variation of the relative intensity of the 220 reflection on changing the amount of one component, we can see whether that component lies on the TPMS or not, because the relative intensity systematically changes with increasing ϕ_L, for example, from Fig. 4(b) to (c).

Fig. 5 plots the relative intensity of the 220 reflection with respect to the 211 reference peak [in terms of $|F(220)|^2/|F(211)|^2$] as a function of n, and the solid line is a guide for the eye. The relative intensity of the 220 reflection decreases with increasing n. This clearly shows that the aliphatic chain part is located on the G-TPMS, because increasing n and increasing the amount of the component on the TPMS (*i.e.* ϕ_L) are certainly parallel. Thus, we have experimentally and for the first time clarified which part (core or aliphatic) of the constituent molecule is located on the G-TPMS in the thermotropic Cub LC systems. Using molecular dynamics simulation, Yoneya *et al.* (2004) proposed a similar picture for BABH-8, although they did not examine the 'core on TPMS' case. On the other hand, some values obtained were beyond the value of 0.433 expected for $\phi_L = 0$. This is probably because the model used is too simple compared with the real system.

The second feature of Fig. 5 is that the *Im*3*m*-phase region exists at around $\phi_L = 0.5$, which is sandwiched by the two *Ia*3*d*-phase regions with $n < 13$ and $n > 16$. We believe that this is a general trend for the thermotropic LC mesogens showing both *Ia*3*d*- and *Im*3*m*-Cub phases, although in the lyotropic LC systems, the lamellar phase is stabilized in that region. This idea is supported by the fact that the

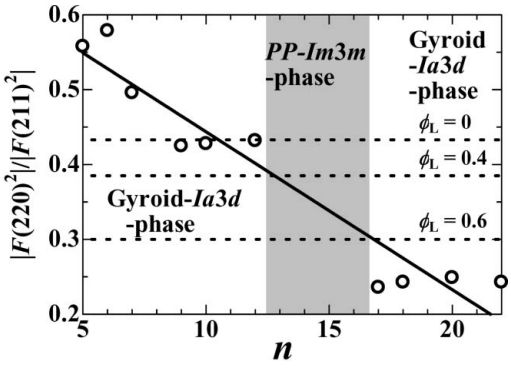

Figure 5
Plots of the relative intensity of the 220 reflection with respect to the 211 reference peak as a function of n, which are compared with three values (broken lines) calculated by Garstecki and Hołyst for $\phi_L = 0$, 0.4 and 0.6; the notations are give in the text. The solid line is a guide for the eye.

Cub phase sequence of *Ia*3*d*–*Im*3*m*–*Ia*3*d* with increasing n is commonly seen for the two thermotropic Cub-phase-forming compounds ANBC-n and BABH-n (Fig. 1).

The third point to note is that the decrease in the relative intensity seems to continue with an intermission of the *Im*3*m*-phase region. If the 'core on TPMS' structure took place at larger n, the thickness of the layer decorating the G surface, and thus ϕ_L, should be reduced with increasing n, leading to an increase of the relative intensity of the 220 reflection. Therefore, the observed trend suggests that the 'chain on TPMS' structure remains stable against a large variation in the chain length (from $n = 5$ to 22!). Such behavior is in striking contrast to lyotropic systems, where two components exchange their roles around $\phi = 0.5$.

It has become evident in this work that the systematic research in terms of the chain length n we have been addressing is useful for clarifying the internal structure of the Cub phases at the molecular level as well as the phase behavior including the Cub phases. Undoubtedly, such research will also contribute to the understanding of factors differentiating between the two thermotropic Cub phases of the *Ia*3*d* and *Im*3*m* types in the near future. Detailed investigations of the Cub phases in the BABH-n series, including, for example, temperature variation of lattice parameters and hydrogen bonding, are certainly worthwhile and are in progress in our laboratories.

We thank Professor Shigeru Okamoto, Nagoya Institute of Technology (Japan), for permission to use his program for converting the two-dimensional IP patterns into circularly averaged ones, Dr Koichi Sakajiri, Gifu University (Japan) for very helpful discussions and Dr Yasuhisa Yamamura, University of Tsukuba (Japan) for helping out with the figures. This work was supported by Grant-in-Aid for Scientific Research (C) 18550121 from Japan Society for the Promotion of Science (JSPS) (SK) and by Grant-in-Aid for Scientific Research (B) 15350110 from JSPS (KS).

References

Clerc, M. & Dubois-Violette, E. (1994). *J. Phys. II Fr.* **4**, 275–286.
Diele, S. (2002). *Curr. Opin. Colloid Interface Sci.* **7**, 333–342.
Diele, S. & Göring, P. (1998). *Thermotropic Cubic Phases*. *Handbook of Liquid Crystals*, Vol. 2B, edited by D. Demus, J. Goodby, G. W. Gray, H.-W. Spiess & V. Vill, pp. 887–900. Weinheim: Wiley–VCH.
Garstecki, P. & Hołyst, R. (2000). *J. Chem. Phys.* **113**, 3772–3779.
Garstecki, P. & Hołyst, R. (2002*a*). *Langmuir*, **18**, 2519–2528.
Garstecki, P. & Hołyst, R. (2002*b*). *Langmuir*, **18**, 2529–2537.
Impéror-Clerc, M. (2005). *Curr. Opin. Colloid Interface Sci.* **9**, 370–376.
International Tables for Crystallography (1989). Volume A, edited by Th. Hahn, second, revised edition. Dordrecht: Kluwer Academic Publishers.
Kutsumizu, S. (2002). *Curr. Opin. Solid State Mater. Sci.* **6**, 537–543.
Kutsumizu, S., Ichikawa, T., Nojima, S. & Yano, S. (1999). *Chem. Commun.* pp. 1181–1182.
Kutsumizu, S., Kato, R., Yamada, M. & Yano, S. (1997). *J. Phys. Chem. B*, **101**, 10666–10673.
Kutsumizu, S., Morita, K., Ichikawa, T., Yano, S., Nojima, S. & Yamaguchi, T. (2002). *Liq. Cryst.* **29**, 1447–1458.
Kutsumizu, S., Morita, K., Yano, S. & Nojima, S. (2002). *Liq. Cryst.* **29**, 1459–1468.
Kutsumizu, S., Yamada, M. & Yano, S. (1994). *Liq. Cryst.* **16**, 1109–1113.
Luzzati, V., Tardieu, A., Gulik-Krzywicki, T., Rivas, E. & Reiss-Husson, F. (1968). *Nature (London)*, **220**, 485–488.
Mori, H., Kutsumizu, S., Ito, T., Fukatami, M., Saito, K., Sakajiri, K. & Moriya, K. (2006). *Chem. Lett.* **35**, 362–363.
Saito, K., Sato, A. & Sorai, M. (1998). *Liq. Cryst.* **25**, 525–530.
Saito, K. & Sorai, M. (2002). *Chem. Phys. Lett.* **366**, 56–61.
Sato, A., Yamamura, Y., Saito, K. & Sorai, M. (1999). *Liq. Cryst.* **26**, 1185–1195.
Schoen, A. H. (1970). NASA Tech. Note No. D-5541, pp. 1–92.
Schubert, H., Hauschild, J., Demus, D. & Hoffmann, S. (1978). *Z. Chem.* **18**, 256.
Schwarz, U. S. & Gompper, G. (1999). *Phys. Rev. E*, **59**, 5528–5541.
Tardieu, A. & Billard, J. (1976). *J. Phys. (Paris) Colloq. C-3*, **37**, 79–81.
Yoneya, M., Nishikawa, E. & Yokoyama, H. (2004). *J. Chem. Phys.* **120**, 3699–3705.
Zeng, X., Ungar, G. & Impéror-Clerc, M. (2005). *Nature Mater.* **4**, 562–567.